Determination of Local Fine Structure of Blood Flows by Measurement Coupled Simulation

Toshiyuki Hayase

Professor
Transdisciplinary Fluid Integration Research Center, Institute of Fluid Science
E-mail: hayase@ifs.tohoku.ac.jp

1. Introduction

Understanding complex blood flows in living bodies is essential to realize advanced diagnosis and treatment for circulatory diseases. The author's group is doing research to analyze complex blood flows by numerical simulation, experimental measurement, and their coupled method in order to determine the local and fine structure of complex blood flows.

This article explains recent research activities of our research group on the measurement coupled simulation of blood flows [1] and the cellular flow in microcirculation [2].

2. Measurement Coupled Simulation of Blood Flows

In order to make accurate diagnosis for cardiovascular diseases, the method to obtain detailed information of the blood flow is essential. Among a number of measurement methods, an ultrasound color Doppler is widely used since it provides a real-time image of the blood flow non-invasively with a relatively compact equipment. However, the velocity measurement with this apparatus provides only the velocity component along the ultrasound beam, and, therefore, it is difficult to comprehend the three-dimensional blood flow.

As a counterpart of measurement, numerical simulation of blood flows has been studied extensively. Realistic solutions of the blood flows are obtained with real vessel geometries obtained with visualizing methods such as CT or MRI. However, the simulation has inherent problem of difficulties in determining computational conditions such as the vessel geometry, inflow and outflow boundary conditions, and the initial condition. The calculated result of the blood flow is usually similar but not exactly identical to the real one.

In order to overcome these problems, we have proposed numerical realization of the blood flow by integrating the ultrasound measurement and the numerical simulation based on the flow observer. Since existing theory of observers is not applicable to complex flow problems, design and evaluation of the feedback schemes were made through numerical experiment in 3-dimensional unsteady problem [1].

2.1. Introduction

Circulatory diseases have been diagnosed considering anatomical abnormalities obtained by medical diagnostic imaging apparatus. Though several empirical indications for specific diseases have been proposed, those criteria are still limited. For the advanced diagnosis, information of blood flow field is essential since hemodynamics such as wall shear stress and pressure distribution on the blood vessel must have close relationships to the development and progress of the diseases. Numerical simulation is capable of providing detailed flow structure [3,4], but there are inherent difficulties in specifying the exact boundary conditions.

In order to overcome the current situation, we have developed a novel numerical simulation of blood flows for diagnosis of circulatory diseases by integrating ultrasonic Doppler measurement on the basis of the concept of flow observer [5]. The method is termed Ultrasonic-Measurement-Integrated (UMI) simulation [6,7]. Figure 1 shows the UMI simulation system for blood flow. In UMI simulation, blood flow is measured by means of color Doppler imaging using ultrasound, and numerical simulation of the targeted blood flow is carried out using estimated computational conditions. During the computational process, feedback signals proportional to the differences between measured and computed results are added to the governing equations in the form of an artificial force term at feedback points defined in the computational domain.

In this paper, we perform a numerical experiment to evaluate UMI simulation of blood flow in a thoracic aneurysm by comparing with an ordinary numerical simulation. A numerical solution obtained by assuming realistic boundary conditions is first defined as a model

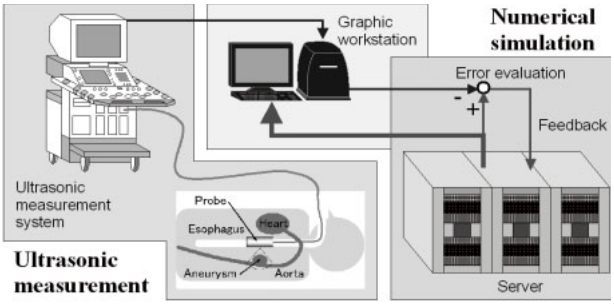

Fig. 1. UMI simulation system for blood flow.

of real blood flow (a standard solution), and then, UMI simulation is investigated concerning the reproduction of the standard solution. In the UMI simulation, boundary condition that is not valid for the standard solution is applied, and feedback signals are generated by comparing measured and computed velocity information. In the measurement, we suppose transesophageal ultrasonic measurement of blood flow in the three-dimensional aneurysmal domain with one probe, which measures only one-directional velocity component along the ultrasonic beam (Doppler velocity).

2.2. Ultrasonic-measurement-integrated (UMI) simulation

Governing equations of UMI simulation are the Navier-Stokes equations for incompressible and viscous fluid flow,

$$\rho\left(\frac{\partial \mathbf{u}}{\partial t}+(\mathbf{u}\cdot\nabla\mathbf{u})\right)=\mu\Delta\mathbf{u}-\nabla p+\mathbf{f}\,, \tag{1}$$

and the pressure equation,

$$\Delta p=-\nabla\cdot\rho(\mathbf{u}\cdot\nabla\mathbf{u})+\nabla\cdot\mathbf{f}\,, \tag{2}$$

where ρ and μ are respectively the density and viscosity of blood, $\mathbf{u}$ = (u, v, w) is the velocity vector, p is the pressure, and $\mathbf{f}$ denotes the body force or the feedback signal. The above described governing equations are discretized by means of the finite volume method. Staggered grid system is introduced for the discretization, and those discretized equations are solved with an algorithm similar to the SIMPLER method [8, 9].

The feedback signal applied at a feedback point is an artificial force proportional to the optimal estimation of the difference in velocity vector obtained by Doppler velocities by ultrasonic measurement and by the UMI simulation as described below:

$$\begin{aligned}\mathbf{f}&=-K_{\mathrm{v}}^{*}\frac{\mathbf{\Phi}_d(\mathbf{u}_{\mathrm{c}}-\mathbf{u}_{\mathrm{s}})}{U}\left(\frac{\rho U^2}{L}\right)\\&=-K_{\mathrm{v}}^{*}\frac{\mathbf{\Phi}_d(\mathbf{u}_{\mathrm{e}})}{U}\left(\frac{\rho U^2}{L}\right)\end{aligned} \tag{3}$$

where K_{v}^{*} is the feedback gain (nondimensional), U is the reference velocity, L is the reference length, $\mathbf{\Phi}_d$ (d = 1, 2, 3) is a projection function of a three-dimensional vector to d-dimensional subspace generated by the vectors of the ultrasonic beam directions, $\mathbf{u}_{\mathrm{c}}$ and $\mathbf{u}_{\mathrm{s}}$ are velocity vectors of computational result and real blood flow, respectively, and $\mathbf{u}_{\mathrm{e}}$ is the error velocity vector. It is noted that ultrasonic measurement provides us a Doppler velocity V_{s}, which is a projection of the velocity vector $\mathbf{u}_{\mathrm{s}}$ onto the ultrasonic beam. Therefore, $\mathbf{u}_{\mathrm{e}}$ and $\mathbf{u}_{\mathrm{s}}$ are unknown, and $\mathbf{\Phi}_d(\mathbf{u}_{\mathrm{e}})$ or $\mathbf{\Phi}_d(\mathbf{u}_{\mathrm{c}}\text{-}\mathbf{u}_{\mathrm{s}})$ is the optimum estimation of them obtained from the measurement data or Doppler velocities.

$$\Phi_d(\mathbf{u}_{\mathrm{e}})=[\mathbf{v}_1\cdots\mathbf{v}_d]\begin{bmatrix}(\mathbf{v}_1,\mathbf{v}_1)\cdots(\mathbf{v}_1,\mathbf{v}_d)\\ \vdots\\ (\mathbf{v}_d,\mathbf{v}_1)\cdots(\mathbf{v}_d,\mathbf{v}_d)\end{bmatrix}^{-1}\begin{bmatrix}V_{\mathrm{e}1}\\ \vdots\\ V_{\mathrm{e}d}\end{bmatrix} \tag{4}$$

where $\mathbf{v}_1$, … , $\mathbf{v}_d$ are the unit vector in the direction of ultrasonic beams, and $V_{\mathrm{e}1}$, … , $V_{\mathrm{e}d}$ are the error of the computed Doppler velocity with respect to that of the measurement. The artificial force $\mathbf{f}$ is decomposed to the three-directional components, f_x, f_y and f_z, and are respectively added to the control volumes of $u(i, j, k)$, $v(i, j, k)$ and $w(i, j, k)$ in the Navier-Stokes equations. Note that the special case with K_{v}^{*} = 0 means the ordinary numerical simulation without feedback.

2.3. Numerical experimentation

The objective flow is blood flow in a descending aorta with an aneurysm. A 76-years-old female patient with a chronic aortic aneurysm in the descending aorta participated in this study. She had no significant cardiac complications. Figure 2(a) shows the full blood vessel configuration with the aneurysm reconstructed from the sliced images acquired by X-ray CT (AquilionTM 16, Toshiba, Tokyo, Japan) by means of commercial three-dimensional reconstruction software (Mimics 7.3, Materialise, Leuven, Belgium), and Table 1 summarizes the patient information obtained in diagnosis. All measurement data were obtained in Tohoku University Hospital.

The computational domain for numerical experiment in this study is represented in Fig. 2(b). The z-axis was defined along the body axis direction, and the x and y-axes were respectively set anterior-posterior and right-left directions. The aneurysm was located in the range of 0.066 m ≤ z ≤ 0.106 m, as shown in Fig. 2(b). The orthogonal equidistant computational grid was generated by introducing a staggered grid system with 43×30×91 grid points in x, y and z directions, respectively. The grid interval h_z in the z-direction was set at 2.00×10^{-3} m, which was the same as the slice interval of X-ray CT used for the acquisition of the blood vessel shape, and those in the other directions were determined $h_x = h_y = 1.79\times10^{-3}$ m, compromising reproducibility of vessel configuration and computational load.

This paper investigates the efficiency of UMI simulation of three-dimensional unsteady blood flow field which is the practical state of real blood flow. A numerical solution with realistic upstream and downstream boundary conditions is first defined as a model of real blood flow instead of the real measurement data which provides only limited information of the real blood flow. In order to specify a realistic boundary condition for the standard solution, a preliminary blood flow simulation in full configuration of Fig. 2(a) was carried out using FLUENT. The computational grid shown in Fig. 2(a) consists of

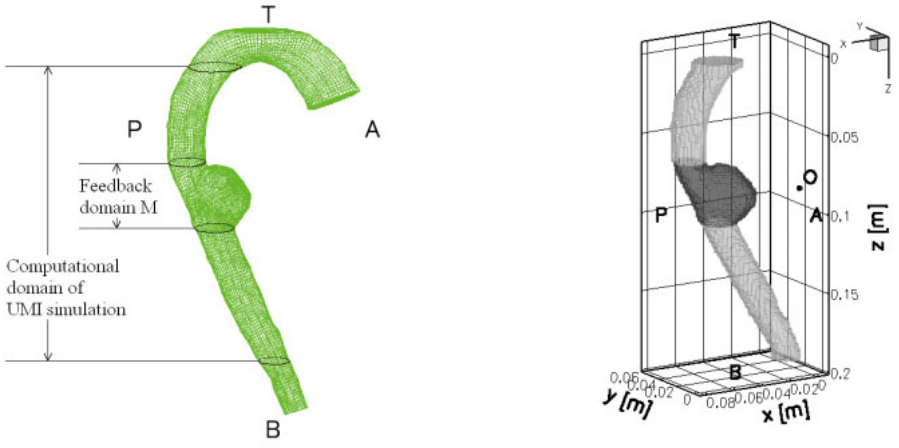

(a) (b)

Fig. 2. Computational domains of (a) whole aorta with an aneurysm for FLUENT and of (b) blood vessel in the vicinity of thoracic aneurysm with feedback domain M and a probe position O for UMI simulation.

142,417 hexahedral elements. The computation was performed with the appropriate computational time increment of 0.01 s. In the computation, an unsteady parallel flow with a uniform velocity profile was applied at the inlet of the ascending aorta. Referring to the MR measurement of the flow rate in an ascending aorta by Olufsen et al. [10] and cardiac output of the patient in this study, the time-variation of flow rate in the one cardiac cycle was obtained at 30 arbitrary timings, as shown in Fig. 3. Note that the total volume of the flow rate was set at 70% of the cardiac output since we deal with the blood flow in the descending aorta only [11]. In practical computation, the flow rate q at each timing of Δt = 0.01 s was calculated by means of the linear interpolation of Fig. 3.

Unsteady calculation was performed in the computational domain of Fig. 2(b). Table 1 summarizes the parameters used in the three-dimensional unsteady blood flow analysis. The unsteady velocity profiles at upstream and downstream boundaries were obtained with reference to the preliminary computational result of steady oscillation in the fourth cardiac cycle by FLUENT. For instance, Fig. 4(a) shows the upstream boundary velocity profiles for the standard solution at three different moments in the acceleration phase (t = 0.06 s), the deceleration phase (t = 0.23 s), and the diastolic phase (t = 0.70 s). At the two phases of t = 0.06 s and 0.23 s in the systole, blood flows fast toward the downstream. The velocity component in the axial direction on the cross-section becomes faster in the distal portion of blood vessel than in the proximal portion because the centrifugal force acts on blood flow in the aortic arch connected to the upstream boundary (see Fig. 2). The velocity profile in the diastolic phase at t = 0.70 s displays swirl which is generated by curvature and torsion of the aorta. Moreover, at the phases t = 0.23 s and 0.70 s, regurgitation can be observed.

Considering that the exact boundary condition of real blood flow field is usually unknown, the UMI simulation is carried out with a boundary condition that is not valid for the standard solution: an unsteady parallel flow with a uniform velocity profile at the inlet and a free flow condition at the outlet with the same flow rate as the standard solution in Fig. 3. Concerning the initial condition, UMI simulation in this study uses a zero velocity field. Though the inaccurate boundary condition introduces error to the blood flow field in the aneurysm, the addition of feedback signals at the feedback points work to reduce the error in the UMI simulation. The feedback points are arranged at all the

Table 1. Computational conditions for three-dimensional unsteady blood flow analysis.

Heat rate	1.02 Hz (61 bpm)
Cardiac cycle T	0.98 s
Cardiac output	7.00×10^{-5} m^3/s (4.2 l/min)
Entrance flow	4.90×10^{-5} m^3/s (2.94 l/min)
Maximum mean velocity u'_{max}	0.37 m/s
Entrance vessel diameter D	29.25×10^{-3} m
Kinematic viscosity ν	4.0×10^{-6} m^2/s

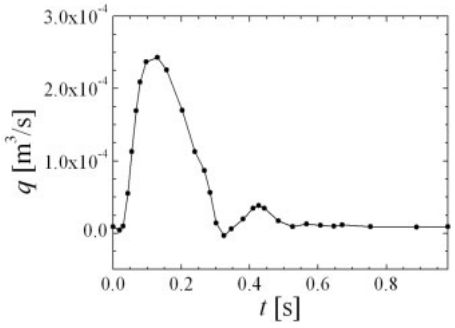

Fig. 3. Time variation of flow rate in an ascending aorta.

grid points in fluid region in the domain M [0.066 m ≤ z ≤ 0.106 m, colored with dark gray in Fig. 2(b)], which covers the whole aneurysmal domain including the parent blood vessel, considering the transesophageal ultrasonography with rotating the probe (see Fig. 1).

It has been revealed that the positioning of one ultrasound probe affects the computational result of UMI simulation using the ultrasound probe and the probe position at the same height of an aneurysm gives the best reduction of the error in velocity field in the aneurysmal domain and fast response to the targeted steady state of blood flow field [12]. Hence, this study performed numerical experiments of UMI simulation of three-dimensional unsteady blood flow, using one probe at the same height of the aneurysm. The one probe is located at the point O [(x, y, z) = (0.014 m, 0.000 m, 0.086 m)] for the acquisition of color Doppler images of the standard solution. Note that aliasing in ultrasonic Doppler measurement is not considered in this study.

The time resolution Δt_{in} of ultrasonic measurement equipment has its own limitation due to the sampling and processing. Therefore, compared to the computational time step Δt, we may not be able to obtain measurement data with an adequate time resolution. However, this study is subject to an ideal condition, or ideal feedback, in which a set of Doppler

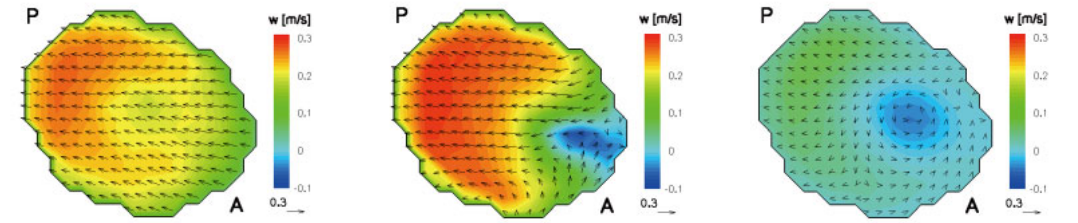

(a) Upstream velocity profiles for the standard solution

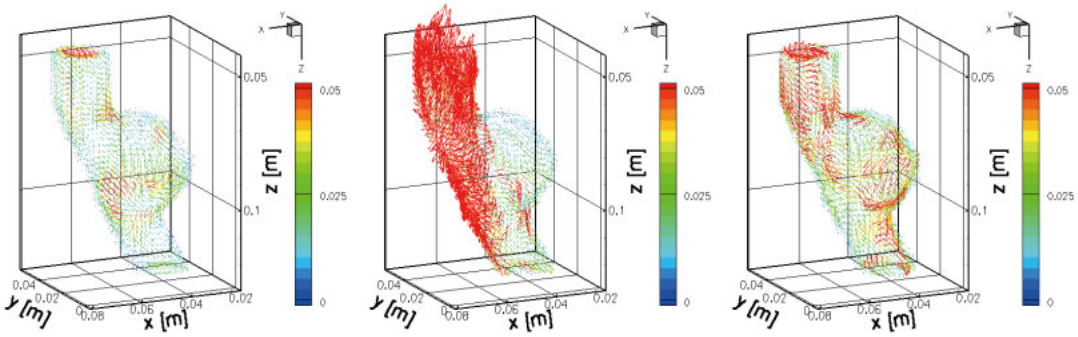

(b) Ordinary simulation

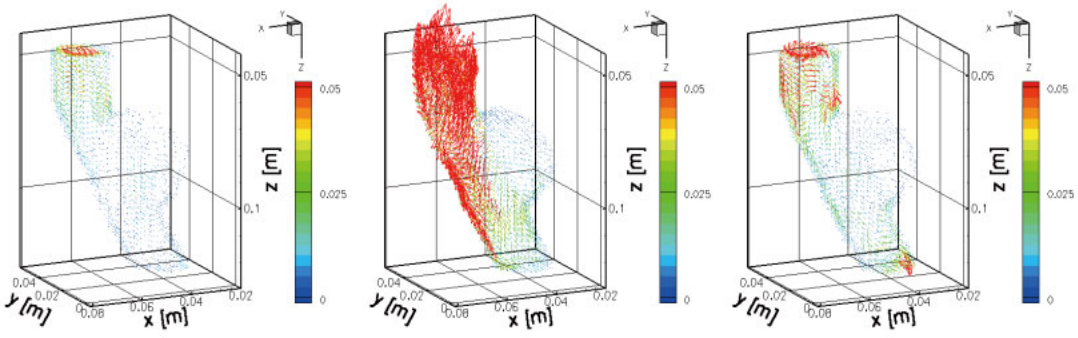

(c) UMI simulation using one ultrasound probe with feedback domain M at $K_v^* = 5$

Fig. 4. Upstream velocity profiles for the standard solution and velocity error vectors (unit: m/s) in the vicinity of the aneurysm of ordinary simulation and UMI simulation using one ultrasound probe at t = 0.06 s in the acceleration phase (left row), at t = 0.23 s in the deceleration phase (middle row), and at t = 0.70 s in the diastolic phase (right row).

velocities is acquired at each computational time step of UMI simulation in order to investigate the efficiency of the UMI simulation for unsteady target flow.

For the evaluation of the computational accuracy, we define the error norm $e_n(a, t)$ of an arbitrary variable at each monitoring point as follows:

$$e_n(a,t) = \frac{|a_{cn}(t) - a_{sn}(t)|}{a_{\text{ref}}} \tag{5}$$

where n is the index point, a is velocity vector $\mathbf{u} = (u, v, w)$ or pressure p, $|\cdot|$ is the absolute value for scalar variables or the l_1 norm, a_{ref} is the characteristic value for normalization: $a_{\text{ref}} = u'_{\max}$ for velocity or $a_{\max} = \rho u'^2_{\max}$ for pressure, and $u'_{\max}$ is the maximum mean flow velocity of the blood at the upstream boundary. Subscript cn corresponds to the computation, i.e., UMI simulation or ordinary simulation, at the grid point with index n, and sn corresponds to the standard solution at the same grid point. By averaging error norms $e_n(a, t)$ over all monitoring points n in a domain Ω, the average error norm $\bar{e}_\Omega(a, t)$ is also defined:

$$\bar{e}_\Omega(a,t) = \frac{1}{N}\sum_{\mathbf{x}_n \in \Omega} e_n(a,t) \tag{6}$$

where N is the total number of the monitoring points in the domain Ω. Here, The domain Ω was arbitrarily chosen for the purpose of evaluation. In this study, all grid points in the fluid region in the feedback domain M are used for $\bar{e}_M(a, t)$. In addition, we use time-averaged value of the average error norm $\bar{e}_{\Omega T}(a)$.

$$\bar{e}_{\Omega T}(a) = \frac{1}{N}\sum_{\mathbf{x}_n \in \Omega} \frac{1}{T}\int_T e_n(a,t)\,dt \tag{7}$$

where T is a duration of one cardiac cycle.

2.4. Results and discussion

After test computation, $K_v^* = 5$ is chosen as the feedback gain of UMI simulation for the improvement of computational accuracy of blood flow field and for computational stability.

Since we assume that the complicated velocity profiles of the standard solution in Fig. 4(a) are unknown and apply a parallel flow with a uniform velocity profile to numerical simulation at each time steps, error is inevitably introduced to the blood flow analysis. Velocity error vectors between the ordinary simulation and the standard solution at the same phases

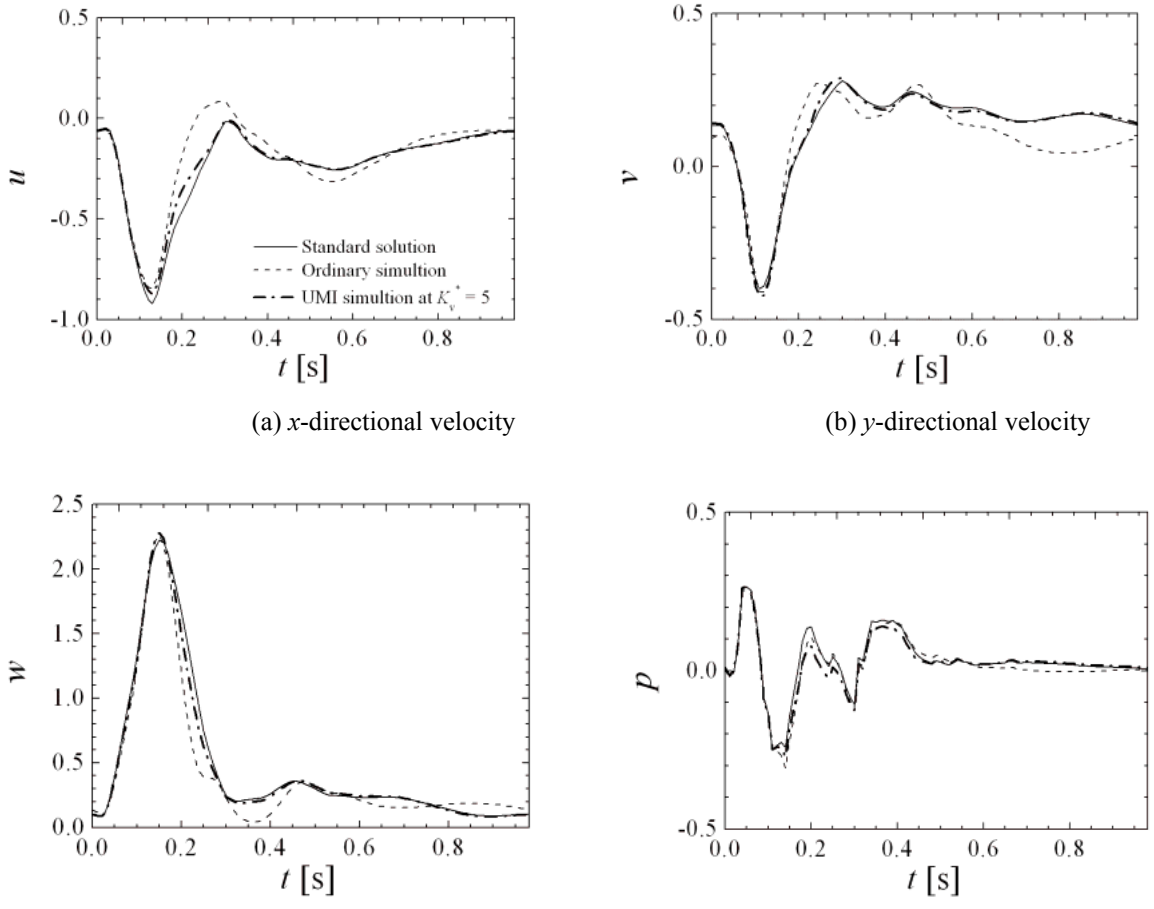

(a) x-directional velocity (b) y-directional velocity

(c) z-directional velocity (d) Pressure

Fig. 5. Comparison of periodic solution of variables at a monitoring point [(x, y, z) = (0.054 m, 0.034 m, 0.086 m)] in the aneurysm among the standard solution, the ordinary simulation and the UMI simulation using one probe (nondimensional).

of Fig. 4(a) are shown in Fig. 4(b). Relatively large error is observed inside the aneurysm where blood flow velocity becomes small because of recirculation. The magnitude of the error vectors becomes large especially in the deceleration phase. This is because the upstream velocity profile becomes the most different in the deceleration phase in the cardiac cycle. In contrast, in the UMI simulation using one probe with feedback domain M [Fig. 4(c)], the velocity error vectors shrinks in and after the aneurysmal domain, which is set as the feedback domain. The magnitude of error vectors in the aneurysm becomes small.

For more detailed observation, Fig. 5 compares the periodic solutions of variables at a monitoring point in the aneurysm [(x, y, z) = (0.054 m, 0.034 m, 0.086 m)] among the standard solution, the ordinary simulation and the UMI simulation. The UMI simulation reduces the error due to the difference in the boundary condition and follows the standard solution, while the ordinary simulation disagrees with the standard solution.

The average error norms, $\bar{e}_{\mathrm{M}}(\mathbf{u},t)$ and $\bar{e}_{\mathrm{M}}(p,t)$, of the velocity vector and the pressure in the aneurysm (feedback domain M) are calculated at each moment as shown in Fig. 6. The ordinary simulation has relatively large error in the deceleration phase ($0.13\ \mathrm{s} \leq t \leq 0.33\ \mathrm{s}$) as indicated by the long velocity error vectors in Fig. 4 (b). The UMI simulations have lower errors than the ordinary simulation at all time steps. The calculation of time-averaged values, $\bar{e}_{\mathrm{M}I}(\mathbf{u})$ and $\bar{e}_{\mathrm{M}I}(p)$, of the average error norms of UMI simulation indicates that the application of feedback in feedback domain M using one probe reduces the error in the aneurysmal domain by a factor of 0.31 for the velocity vector and 0.53 for the pressure in one cardiac cycle. Hence, it is confirmed that the error in the velocity field becomes small.

In order to investigate the effectiveness of UMI simulation for providing information of hemodynamic stresses on blood vessel for advanced medical diagnosis of circulatory diseases, wall shear stress distribution is calculated by first-order numerical differentiation of the velocity vectors. Figure 7 compares the time-averaged wall shear stress distribution among the standard solution, the ordinary simulation and the UMI simulation. All simulations show similar distributions, however the ordinary simulation tends to estimate lower wall shear stress in the aneurysm. The UMI simulation displays a similar distribution as the ordinary simulation in the upstream domain but accurately provides the wall shear stress distribution of the standard solution in the aneurysm. In each figure in Fig. 7, a white dot represents the position of the large value of the time-averaged wall shear stress at the aneurysmal neck. The ordinary simulation reproduces the positions of the large wall shear stress, but the values are 9% lower in Fig. 7(a) and 16% higher in Fig. 7(b) than that of the standard solution, respectively. In comparison, the UMI simulation reproduces both the proper position and the value with only 1% deviance. Hence, UMI simulation can produce more reliable information of hemodynamic stresses than the ordinary simulation. Note that the ordinary simulation provides a similar blood flow field to the standard solution on the whole but sometimes shows local disagreements, which may cause a big mistake in the diagnosis of circulatory diseases.

2.5. Conclusions

The potential of UMI simulation to accurately reproduce real blood flows have been validated by a numerical experiment dealing with the three-dimensional unsteady blood flow field in an aneurysmal aorta. The feedback of the optimal estimation of difference in velocity vector against real blood flow obtained by ultrasonic measurement using one probe decreases the errors due to inaccurate boundary condition in velocity and pressure decrease to 31% and to 53%, respectively, in the aneurysmal domain. UMI simulation of real blood flows will bring significant benefits for the clinical diagnosis and treatment of circulatory diseases: the detailed and accurate information of blood flows is provided and hemodynamic stresses are more correctly estimated than by existing methods.

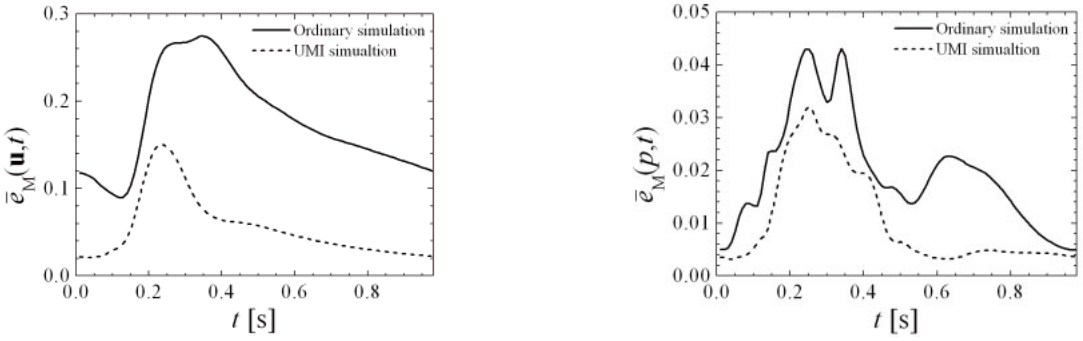

(a) Velocity vector (b) Pressure

Fig. 6. Time-variations of average error norms of velocity vector and pressure in the aneurysm of the ordinary simulation and the UMI simulation using one probe.

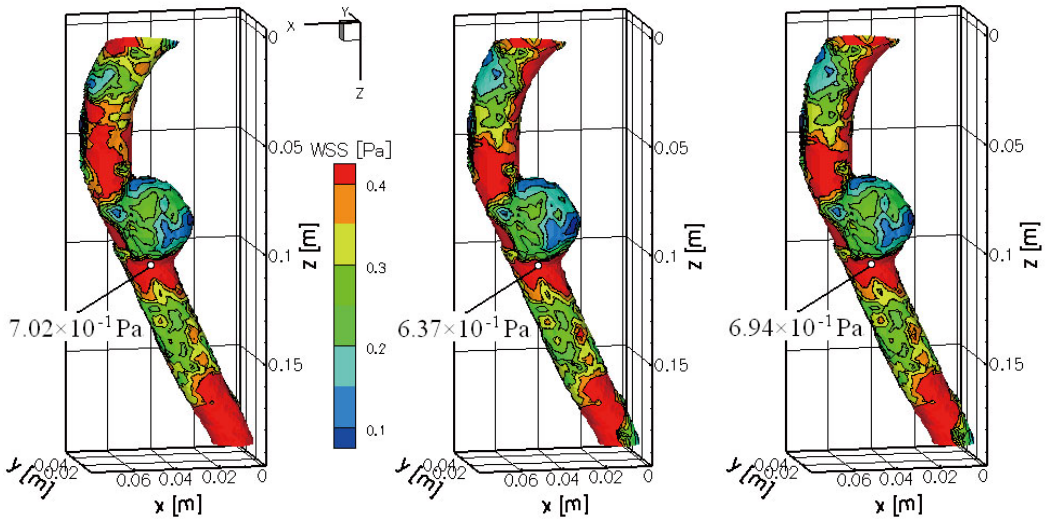

(a) Right view

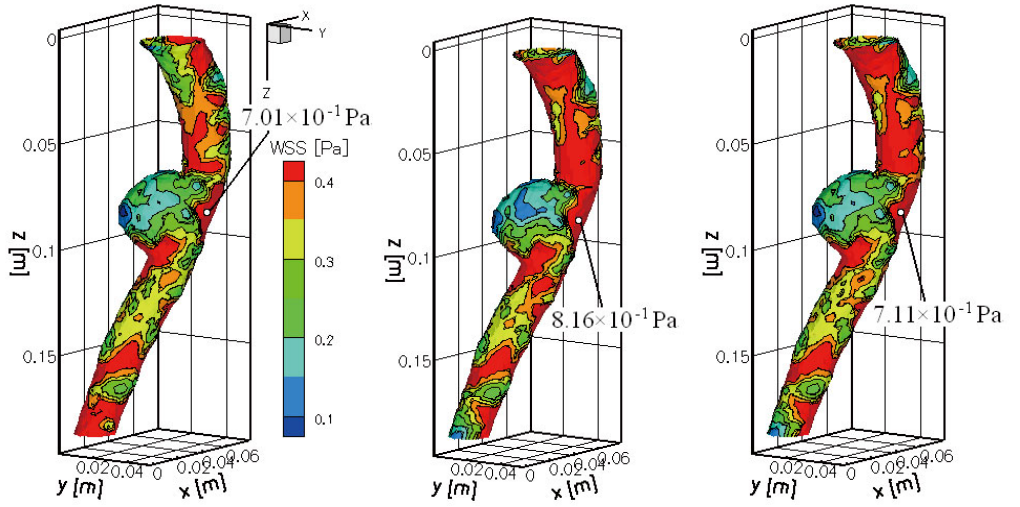

(b) Left view

Fig. 7. Comparison of time-averaged wall shear stress on the blood vessel among the standard solution (left row), the ordinary simulation (middle row) and the UMI simulation using one probe (right row). Each white dot implies large value of wall shear stress at the aneurysmal neck.

3. Cellular Flow in Microcirculation

As a fundamental research for modeling of microcirculation, frictional characteristics of blood cells on a glass plate are investigated with an inclined centrifuge microscope [2].

3.1. Introduction

Blood flow in microcirculation plays an important role in supplying tissues with nutrients and removing metastases. Extensive physiological research has been carried out to examine blood flow in microcirculation [13], focusing on the complex interaction between blood cells, plasma proteins, and glycocalyx in the layer on the surface of endothelial cells [14]. The lack of direct measurements to verify these results is a critical problem in the study of microcirculation.

Harvey [15] invented the centrifuge microscope which enables us to observe cells under centrifugal force, and, to date, several different types of centrifuge microscope have been developed [16]. However, all existing centrifuge microscopes are designed such that the direction of cell deformation or movement and the direction of the centrifugal force are identical. Therefore, the magnitude of the centrifugal force is the only parameter to be specified (see Fig. 8 (a)). The present study involves the *inclined centrifuge microscope* developed by the author [17] which enables cells on an inclined plate to be observed under centrifugal force while specifying the tangential and normal force

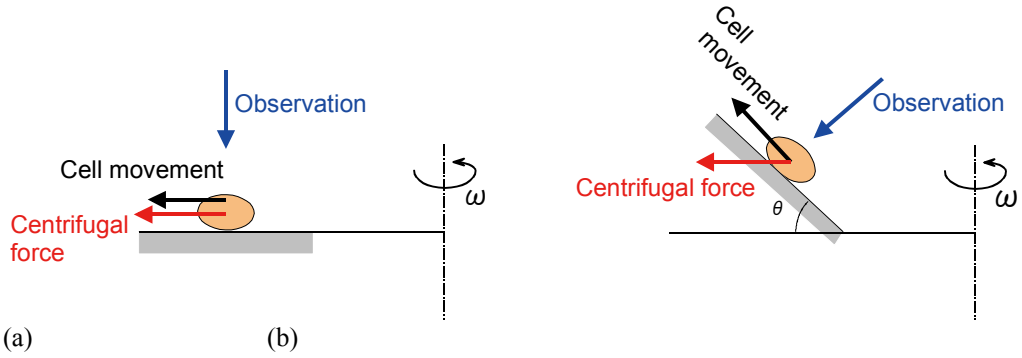

Fig. 8. Conventional and inclined centrifuge microscopes: (a) conventional, (b) inclined

components independently (Fig. 8 (b)). In order to gain a fundamental understanding of the blood cell interaction mentioned above, the present study investigates the measurement of the frictional characteristics of red blood cells moving along a glass plate in a plasma using the inclined centrifuge microscope.

3.2. Materials and methods

As a sample, human venous blood was anticoagulated by citric acid sodium, and centrifuged (1,000 g, 10 min). Red blood cells were distributed in the plasma at a volumetric concentration of 0.05%.

A cover glass (Takahashi Giken Glass) degreased via ethylalcohol was used as the base plate on which the frictional force of the red blood cell was measured.

A schematic diagram of the experimental system is shown in Fig. 9. A newly developed *inclined centrifuge microscope* is the primary component of the equipment. A pair of inclined containers of inner dimension of 10 mm × 8 mm × 1 mm (width × length × height) is mounted on the rotor of a centrifuge (KUBOTA, Model 1120). One of the two containers is filled with the sample fluid while the other container remains empty. The rotation speed of the rotor is measured using a digital tachometer (ONO SOKKI, TM-2110, accuracy: 0.02%). A reference signal synchronizing with the rotation, which is generated by a laser diode and a detector and delayed through a pulse generator, triggers a pulse laser diode (NEO ARK, PLD-9010, wavelength: 900 nm, peak power: 20 W, half width: 50 ns). The laser beam, which is guided through an optical fiber (NIKON, GFLG-5), illuminates the container filled with the sample fluid for a very short interval of 50 ns at the same angular position of the spinning rotor so that a still figure of the container can be observed. Red blood cells moving on the base plate are observed through a microscope (NIKON, CM-10M, objective: OLYMPUS Cplan FI 10X), which is rotated with an angle normal to the base plate. The image of the blood cell movement is recorded using a CCD camera (IKEGAMI, SKC-141 145 M pixels) and a PC.

A schematic diagram of the sample container is shown in Fig. 10. The base plate is placed at the bottom of the container, which is inclined at an angle of θ from

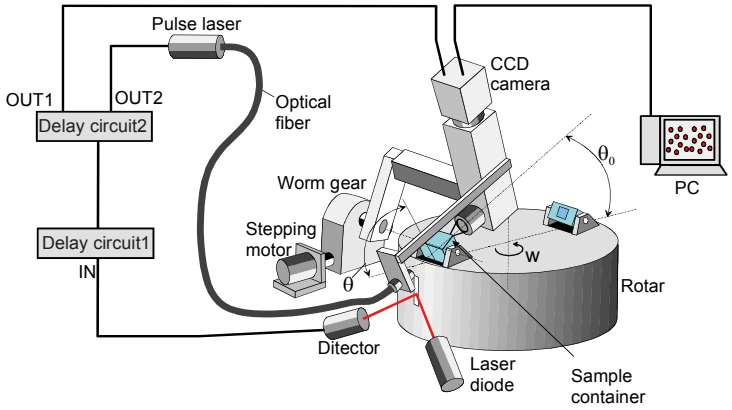

Fig. 9. Schematic diagram of the experimental system

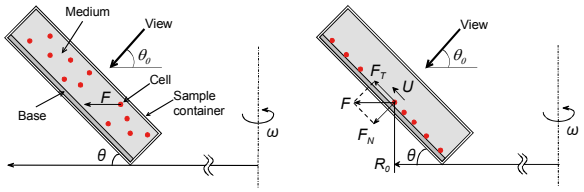

(a) **(b)**

Fig. 10. Principle of frictional force measurement in a rotating field: (a) initial state, (b) steady-state movement of red blood cells

the horizontal plane (Fig. 10 (a)). The container is filled with plasma in which red blood cells have been dispersed. By applying rotation at an angular velocity ω, the cells move in the radial direction under the effect of centrifugal force *F*. After cells contact the base plate, the centrifugal force on each cell is naturally divided into two components; the normal force F_N and the thrust force F_T (Fig. 10 (b)). The normal force F_N balances the reaction from the base plate, and the thrust force F_T accelerates the cell along the base plate. When the cell velocity U reaches a steady value, the thrust force F_T is equal to the sum of the frictional force F_T* from the base plate and the drag force f_D from the medium above the cell. Since the force components F_N and F_T are specified arbitrarily by adjusting the angle of the container θ and the angular velocity ω, measuring the cell velocity U for a variety of force conditions gives the frictional characteristics of the red blood cells moving along the base plate.

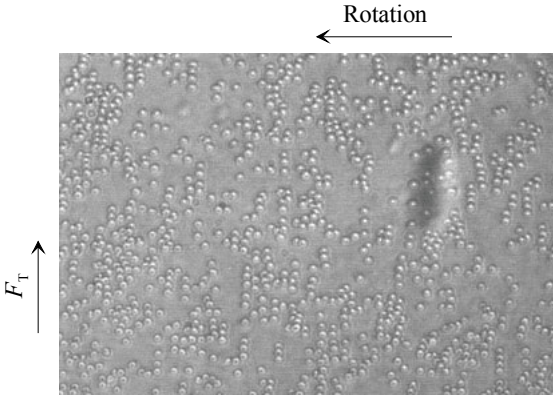

Fig. 11. Red blood cells moving on a glass plate in plasma

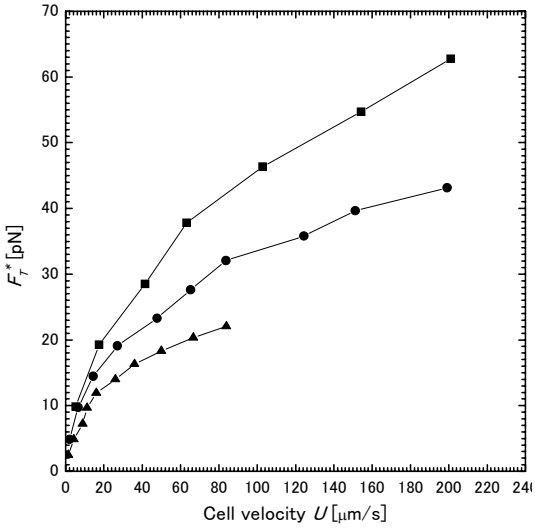

Fig. 12. Frictional characteristics of red blood cells moving on a glass plate in plasma

Measurement of cell velocity was performed by a particle tracing velocimetry (PTV) software (NEXUS,PIV expert 2000). The image processing was performed using up to 300 frames at arbitrary time intervals. Each image consists of 1392 × 1040 pixels with 256-level monochrome gradation and a diameter of 0.64 μm. After removal of background noise and smoothing, the centers of gravity of all red blood cells were obtained. The particle tracing velocimetry method was then applied in order to determine the velocity vectors of all cells based on the distributions of cell centers at two times.

3.3. Results and discussion

The experiment was performed under the condition in which the thrust force F_T was varied while the normal force F_N remained constant. Temperature was maintained constant at 25±1°C during the experiment.

Figure 11 shows a part of the frame obtained in the experiment. Small circles are red blood cells moving on a glass plate in plasma by the effect of inclined centrifugal force.

Figure 12 shows the resultant frictional characteristics of red blood cells. The figure contains the results for three values of the normal force F_N. Each point represents the mean value for four measurements each of which has more than 1000 data.

Measured result reveals the nonlinear frictional characteristics. The friction force is appropriately represented as the viscous friction for the cell velocity up to 20 μm/s, but increase rate of the friction becomes smaller in larger cell velocity region.

4. Conclusions

The author's group is doing research to analyze complex blood flows by numerical simulation, experimental measurement, and their coupled method. The coupled method enables us to perform a highly accurate and high speed analysis of the local and fine structure of complex blood flows.

References

[1] Funamoto K, Hayase T, Saijo Y, and Yambe T. Accuracy of ultrasonic-measurement-integrated simulation for three-dimensional blood flow in aneurysmal aorta. *Proceedings of the 5th Joint ASME/JSME Fluids Engineering Conference*, FEDSM2007, 1-6 (CDROM), 2007.

[2] Hayase T, Sugiyama H, Yamagata T, Inoue K, Shirai A, and Takeda M. Inclined Centrifuge Microscope For Measuring Frictional Characteristics Of Red Blood Cells Moving On Glass Plate In Plasma. *Proceedings of the 2005 Summer Bioengineering Conference*, CD-ROM, 1-2, 2005.

[3] Steinman DA. Image-Based Computational Fluid Dynamics Modeling in Realistic Arterial Geometries. *Ann Biomed Eng* **30**, 483-497, 2002.

[4] Di Martino ES, Guadagni G, Fumero A, Ballerini G, Spirito R, Biglioli P, and Redaelli A. Fluid-Structure Interaction within Realistic Three-Dimensional Models of the Aneurysmatic Aorta as a Guidance to Assess the Risk of Rupture of the Aneurysm. *Med Eng Phys* **23**, 647-655, 2001.

[5] Hayase T and Hayashi S. State Estimator of Flow as an Integrated Computational Method with the Feedback of Online Experimental Measurement. *J Fluid Eng-T Asme* **119**, 814-822, 1997.

[6] Funamoto K, Hayase T, Saijo Y, and Yambe T. Numerical Study on Variation of Feedback Methods in Ultrasonic-Measurement-Integrated Simulation of Blood Flow in the Aneurysmal Aorta. *JSME Int J Ser C* **49**, 144-155, 2006.

[7] Funamoto K, Hayase T, Shirai A, Saijo Y, and Yambe T. Fundamental Study of Ultrasonic-Measurement-Integrated Simulation of Real Blood Flow in the Aorta. *Ann Biomed Eng* **33**, 415-428, 2005.

[8] Patankar SV. *Numerical Heat Transfer and Fluid Flow*. Hemisphere Pub. Corp, Washington DC/New York, 1980.

[9] Hayase T, Humphrey JAC, and Greif R. Mini-Manual for ROTFLO2. *Dept Mech Eng Rep* **FM-90-1**, Univ. Calif, Berkeley, 1990.

[10] Olufsen MS, Peskin CS, Kim WY, Pedersen EM, Nadim A, and Larsen J. Numerical Simulation and Experimental Validation of Blood Flow in Arteries with Structured-Tree Outflow Conditions. *Ann Biomed Eng* **28**, 1281-1299, 2000.

[11] Ganong WF. *Review of Medical Physiology.* Appleton & Lange, *Norwalk*, 1995.

[12] Funamoto K, Hayase T, Saijo Y, and Yambe T. Effect of Ultrasound Probe Placement in Ultrasonic-Measurement-Integrated Simulation of Blood Flows. *Proc ICBME2005*, CD-ROM, 2005.

[13] Schmid-Schoenbein GW. Biomechanics of microcirculatory blood perfusion. *Annu Rev Biomed Eng* **1**, 103-127, 1999.

[14] Pries AR, Secomb TW, and Gaehtgens P. The endothelial surface layer. *European Journal of Physiology* **440**, 653-666, 2000.

[15] Harvey EN and Loomis AL. Scientific apparatus and laboratory methods. *Science* **72**, 42-44, 1930.

[16] Inoue S, Knudson RA, Goda M, Suzuki K, Nagano C, Okada N, Yakahashi H, Ichie K, Iida M, and Yamanaka K. Centrifuge polarizing microscope. I. Rationale, design and instrument performance. *Journal of Microscopy*, 201-3, 341-356, 2001.

[17] Hayase T, Shirai A, Sugiyama H, and Hamaya T. Measurement of frictional characteristics of red blood cells moving on a plate in plasma due to inclined centrifugal force. *Trans Japan Soc Mech Eng* **68**, 3386-3391, 2002 (in Japanese).